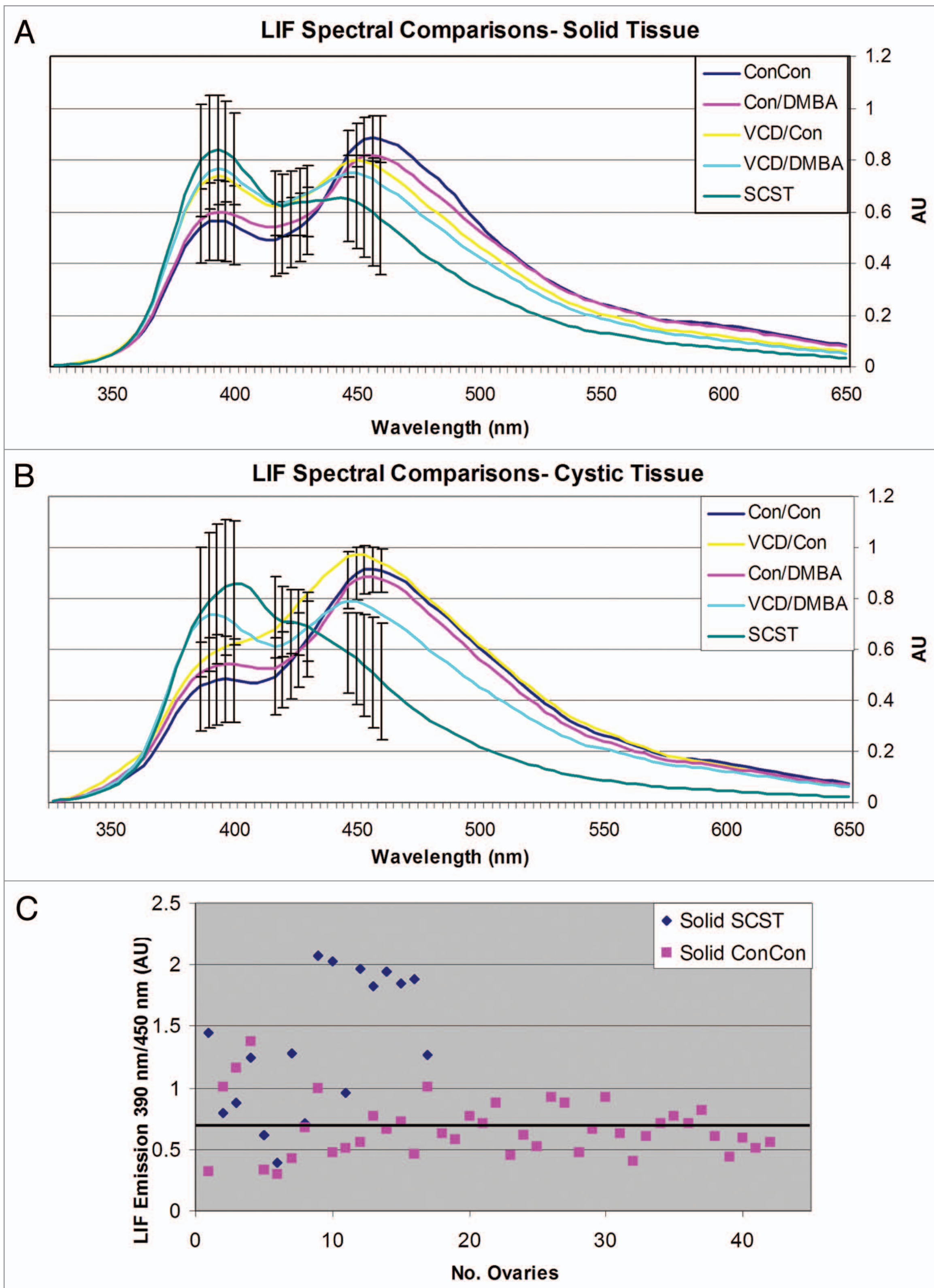

Figure 5. LIF spectral curves. (A) Solid tissue spectral curves. (B) Cystic tissue spectral curves. (C) Scatterplot of the ratio of 390 nm to 450 nm fluorescence emission compared among solid regions of ConCon normal cycling ovaries and solid SCST. Using a cut-off of 0.7 AU (black bar), a sensitivity of 88% to SCST and a specificity of 60% to normal cycling ovaries is achieved. AU: Arbitrary units. No.: Number.

Table 3. LIF spectral comparisons

Tissue at 390 nm em	Solid p-value	Cystic p value
ConCon vs. SCST	0.0026	0.0268
ConDMBA vs. SCST	0.0076	<0.001
ConDMBA vs. VCD DMBA	0.0248	0.049
ConCon vs. ConDMBA	>0.05	>0.05
ConCon vs. VCDCon	0.0242	>0.05
ConCon vs. VCD DMBA	0.0065	0.0126
Tissue at 420 nm em		
ConCon vs. SCST	0.0307	0.015
ConDMBA vs. SCST	>0.05	0.048
ConDMBA vs. VCDCon	>0.05	0.041
ConDMBA vs. VCD DMBA	0.0487	>0.05
ConCon vs. VCDCon	0.0051	0.0115
ConCon vs. VCD DMBA	0.0011	>0.05
Tissue at 450 nm em		
ConCon vs. SCST	0.012	0.0002
ConDMBA vs. SCST	0.0354	0.0017
VCDCon vs. SCST	0.0422	0.0018
VCD DMBA vs. SCST	>0.05	>0.05
ConCon vs. VCD DMBA	0.0395	>0.05

em, emission.

©2010 Landes Bioscience.
Do not distribute.

tissue and neoplasms,[16,34] but are inconsistent with the results found in a prior study of fluorescence spectroscopy in a VCD/DMBA treated rat ovarian carcinogenesis model[35] and previous studies of fluorescence spectroscopy in other types of neoplastic tissues, including cervix, colon and bladder,[27] both of which report neoplastic tissues as generally characterized by a relative increase in 450 nm emission due to increased metabolic activity and a relative decrease in 390 nm emission from collagen. Sex cord-stromal tumors have a thin collagenous capsule surrounding the neoplastic mass, which may be the source for the increased 390 nm emission. Second harmonic generation studies of the ovary show an increase in collagen as well as a change in collagen crosslinking which gives an increased signal from collagen and may also be found here.[39] These tumors are characterized as slow growing neoplasms, which may result in decreased metabolic activity and a relative decrease in 450 nm emission from NADH, specifically when compared with metabolically active cycling ovaries.

Differentiating normal follicles, epithelial inclusions and cystic SCST will also be crucial. Given the small size of most epithelial inclusions and the large spot size of the fluorescence excitation beam, we are unable to evaluate if these entities can be distinguished by fluorescence spectroscopy. Future studies will utilize focused-beam fluorescence spectroscopy to evaluate if epithelial inclusions can be distinguished from follicles and cystic neoplasms.

In previous studies of fluorescence spectroscopy in VCD/DMBA treated rat models, DMBA exposure was accomplished by introducing a DMBA soaked suture into the ovary. This resulted in a significant inflammatory reaction which may have resulted in a higher 450 nm emission peak from the metabolic activity of the inflammatory cells. Additionally, the number of tumors in the previous fluorescence spectroscopy study of the VCD/DMBA ovarian carcinogenesis model were small (n = 3) and were a mix of epithelial and stromal tumors, which may also account for the discrepancy in fluorescence signatures.[35] Future studies will be aimed at further characterizing the fluorescence signature of larger numbers of a variety of ovarian neoplasms.

The vast majority of human ovarian malignancies are epithelial in origin.[1] The animal model used in this study expressed stromal ovarian neoplasms, specifically SCST which represent <0.5% of human ovarian malignancies.[40] There is a very large difference between the two forms of ovarian malignancy in stage at time of diagnosis; greater than 75% of epithelial ovarian neoplasms are stage III or IV at the time of diagnosis, but approximately 70% of stromal ovarian neoplasms are at stage I at the time of diagnosis due to more specific symptomology from neoplasm hormone production.[1,40] Although this is a relatively rare cancer, the ability to distinguish an ovarian cancer from benign ovary would have significant clinical utility, particularly if it was confined to the ovary. To date no reliable rodent model of human ovarian cancer exists, so the availability of a rat model capable of providing reliable stromal tumors may be useful in characterizing the pathogenesis of these tumor types. The successful application of OCT-LIF to a rodent model of ovarian cancer providing preliminary imaging criteria to differentiate cyclic ovaries mimicking pre-menopausal human females, acyclic ovaries mimicking post-menopausal human females, and stromal neoplasms is encouraging and should also be applicable to other types of ovarian tumors as it has been evaluated in previous imaging of human epithelial ovarian carcinoma.[2,16] Future studies will evaluate additional animal models with the intent to develop a model for epithelial ovarian cancer. Additionally, as this was a pilot study, the bilateral ovaries of a single animal were included in a given treatment group despite the fact that only the right ovary was treated with saline or DMBA, unless the ovary was found to be neoplastic, in which case it was assigned to the neoplasm group. Histological evaluation and OCT imaging showed no structural differences between the bilateral ovaries of a single rat, indicating that although the treatment was directly applied to the right ovary, the effects of the treatment appear to be systemic. However, in future studies we will treat the bilateral ovaries as dependent but separate in analysis to determine if direct treatment of one ovary has equal effects on the bilateral, untreated ovary.

An additional limitation to this study was the large spot size of the fluorescence incident light (1.25 mm) compared to the OCT lateral resolution (18 μm). Due to this discrepancy, the data are not directly comparable as the fluorescence data encompasses a much larger tissue volume than is depicted in the OCT images. Future studies will be aimed at developing focused OCT-LIF probes such that direct comparisons between OCT and LIF data can be reliably performed.

In this study, we present the successful implementation of combined OCT-LIF to image a post-menopausal rat model of ovarian stromal cancer. Comparison of OCT images and corresponding histopathology allowed for the description of (1)

preliminary microstructural features of normal cyclic ovary including follicles, CL and CL remnants, (2) features of acyclic ovaries including presence of degenerating follicles, increases in stromal collagen, presence of epithelial invaginations/inclusions and vascular changes associated with VCD and DMBA treatment and (3) features of both solid and cystic SCSTs. LIF was able to characterize spectral differences in fluorescence emission attributed to collagen, NADH/FAD and hemoglobin absorption among cyclic ovaries, acyclic ovaries and SCSTs. Additionally, future ex vivo and in vivo imaging will evaluate a finer disease spectrum including normal ovary, benign cyst (simple and inclusion), cyst adenoma, borderline tumors and malignant neoplasms of epithelial origin in addition to neoplasms of stromal and germ cell origin to develop more concrete qualitative and quantitative criteria to aid with differentiation of these entities.

Materials and Methods

Animals. Eighty three female Fisher-344 rats (age d21, Harlan Sprague Dawley) were housed by the University of Arizona Animal Care in microisolators on a 12:12 hr light/dark cycle, constant temperature and humidity, and free access to food and water per NIH guidelines and the policies of the University of Arizona Institutional Animal Care and Use Committee. The animals were allowed a seven day acclimation period before the initiating the experiment. Protocols were approved by the University of Arizona Institutional Animal Care and Use Committee.

©2010 Landes Bioscience. Do not distribute.

VCD treatment. Day 28 old rats received daily (25 d) i.p. injection with either sesame oil vehicle (2.5 ml/kg, Sigma Chemical Company, St. Louis, MO) or VCD (160 mg/kg, Sigma Chemical Company, St. Louis MO).

DMBA treatment. Four months subsequent to the end of VCD dosing, rats (n = 9–14/treatment-timepoint) received a single injection of either sesame oil (vehicle) or DMBA (100 μg DMBA in 10 μl, Sigma Chemical Company, St. Louis MO) under the bursa of the right ovary using a surgical approach.[2] This method was chosen to eliminate the foreign body response possibly caused by an indwelling suture, and preferentially expose the ovarian epithelium to DMBA. Anesthesia was achieved by i.p. injection of 2% Avertin (stock solution: 25 gm tribromoethanol in 15.5 ml 2-butanol; 2 ml stock in 100 ml sterile saline, Aldrich Chemical Company, St. Louis MO). The left ovary was not injected, serving as an internal control.

Animal grouping. Rats were assigned to one of four experimental groups (**Table 1**). Con/Con group (n = 22) received sesame oil by i.p. injection (2.5 ml/kg/day; 25 d) and a single ovarian injection of sesame oil (10 μl) four months after the end of i.p. sesame oil dosing. VCD/Con (n = 18) received VCD (160 mg/kg/day i.p.; 25 d) and a single ovarian injection of sesame oil four months after VCD dosing was completed. Con/DMBA (n = 17) received sesame oil by i.p. injection (25 d) and a single ovarian injection of DMBA (100 μg in 10 μl) four months after the end of sesame oil dosing. VCD/DMBA (n = 26) received VCD (25 d) and a single ovarian injection of DMBA four months after VCD dosing was completed. Ovaries were collected three (n = 8–12/treatment) or five (n = 9–14/treatment) months post-surgery (seven or nine months, respectively, after the end of i.p. VCD or sesame oil dosing).

Optical imaging. Ovaries were harvested at three or five months post DMBA treatment and imaged using a 2-mm diameter side-firing catheter that optically combined both the OCT and LIF subsystems, previously described in detail.[36] The OCT subsystem used a superluminescent diode source with a 1,300 nm center wavelength (D1300-HP, Superlum, Moscow, Russia) with axial and lateral resolutions of approximately 14 μm and 18 μm, respectively. The LIF subsystem used a helium cadmium laser source (Kimmon Electric, Englewood, Colorado) with a 325 nm excitation wavelength, which was chosen due to its ability to excite endogenous fluorophores NADH, FAD and collagen. Excitation light was delivered with a single multimode fiber and fluorescence emission was collected using two separate multimode fibers directed to a spectrometer equipped with a cooled charge-coupled device. The excitation power was 500 μW and integration time was 1 second. The illumination spot size was 1.25 mm. The cut off wavelength of the long pass filter was 50% transmission at 350 nm.

The OCT beam reached focus at 300 microns outside the catheter envelope and the LIF spot size at the corresponding depth was approximately 1 mm. The excitation light power on the tissue was 0.2 mW and the radiant exposure was 0.22 J/cm 2, both within American National Standards Institute maximal permissible exposure levels.

OCT images 6–8 mm lateral by 1.4 mm deep and approximately 5 corresponding LIF spectra/mm in the lateral dimension were acquired simultaneously at 625 μm increments across the dorsal surface of an ovary. A coupling agent (water-based, non-fluorescent lubricant) was used between the catheter and ovary to decrease backreflection from the air-tissue boundary. Data were acquired by a computer and analyzed using Matlab (The Math-Works, Natick, Massachusetts). Time from ovary excision to completion of imaging was less than 30 minutes.

Histology. Ovaries were fixed in Bouin's solution for 2–4 hours, transferred to 70% ethanol, dehydrated, embedded in paraffin blocks and sectioned (5 μm thickness). Every 20th section was mounted and stained with hematoxylin and eosin (H & E).

Optical image analysis. For each animal group (Con/Con, VCD/Con, Con/DMBA and VCD/DMBA), portions of each OCT image and corresponding LIF spectra were classified into one of five histologically confirmed tissue categories: (1) bursal fat, (2) normal cyclic, (3) normal acyclic, (4) benign cyst or (5) neoplastic ovary. OCT images were compared with corresponding histology to identify architectural features associated with each of the above tissue categories. The average maximum fluorescence value was calculated among all spectra. Fluorescence spectra with maximum fluorescence values <10% of the average maximum fluorescence value were removed from analysis due to spectra being low intensity (approximately 3.5% of total fluorescence spectra). LIF spectra were peak normalized and the mean spectra were compared between animal groups/tissue categories. Statistical differences were determined using the Student's t-test. Particular attention was paid to emission peaks at 390 and 450 nm (generally associated with collagen and NADH, respectively) and a dip

at 420 nm (associated with hemoglobin absorption). Because the LIF spectra are highly overlapping and are thus not independent, *N* in the statistical analysis was chosen to be the total number of ovaries in each group from which spectra were compiled.

Signal attenuation comparison analysis. OCT signal attenuation was compared between regions of interest containing histologically confirmed corpora lutea (CL, n = 32 CL in 32 Con/Con ovaries, one corpus luteum per ovary) and solid neoplasms (n = 12 tumors in 12 ovaries, one tumor per ovary). The surface of each structure was manually defined and the image was flattened to the assigned surface. All image columns were averaged and linear fit to the grayscale intensity. Slopes of the intensity decay profiles were averaged over all CL and neoplasms and compared with the one-tailed Student's t-test.

Acknowledgements

These studies were supported by R01s CA119200 (J.K.B) and AG021948 (P.B.H).

References

1. Cancer Facts and Figures. In: American Cancer Society; 2008.
2. Hoyer PB, Davis JR, Bedrnicek JB, Marion SL, Christian PJ, Barton JK, et al. Ovarian neoplasm development by 7,12-dimethylbenz[a]anthracene (DMBA) in a chemically-induced rat model of ovarian failure. Gynecol Oncol 2009; 112:610-5.
3. Kao SW, Sipes IG, Hoyer PB. Early effects of ovotoxicity induced by 4-vinylcyclohexene diepoxide in rats and mice. Reprod Toxicol 1999; 13:67-75.
4. Springer LN, McAsey ME, Flaws JA, Tilly JL, Sipes IG, Hoyer PB. Involvement of apoptosis in 4-vinylcyclohexene diepoxide-induced ovotoxicity in rats. Toxicol Appl Pharmacol 1996; 139:394-401.
5. Hu X, Flaws JA, Sipes IG, Hoyer PB. Activation of mitogen-activated protein kinases and AP-1 transcription factor in ovotoxicity induced by 4-vinylcyclohexene diepoxide in rats. Biol Reprod 2002; 67:718-24.
6. Stewart SL, Querec TD, Ochman AR, Gruver BN, Bao R, Babb JS, et al. Characterization of a carcinogenesis rat model of ovarian preneoplasia and neoplasia. Cancer Res 2004; 64:8177-83.
7. Ting AY, Kimler BF, Fabian CJ, Petroff BK. Characterization of a preclinical model of simultaneous breast and ovarian cancer progression. Carcinogenesis 2007; 28:130-5.
8. Nishida T, Sugiyama T, Kataoka A, Ushijima K, Yakushiji M. Histologic characterization of rat ovarian carcinoma induced by intraovarian insertion of a 7,12-dimethylbenz[a]anthracene-coated suture: common epithelial tumors of the ovary in rats? Cancer 1998; 83:965-70.
9. Crist KA, Zhang Z, You M, Gunning WT, Conran PB, Steele VE, et al. Characterization of rat ovarian adenocarcinomas developed in response to direct instillation of 7,12-dimethylbenz[a]anthracene (DMBA) coated suture. Carcinogenesis 2005; 26:951-7.
10. Tanaka T, Kohno H, Suzuki R, Sugie S. Lack of modifying effects of an estrogenic compound atrazine on 7,12-dimethylbenz(a)anthracene-induced ovarian carcinogenesis in rats. Cancer Lett 2004; 210:129-37.
11. Drexler W. Cellular and functional optical coherence tomography of the human retina: the Cogan lecture. Invest Ophthalmol Vis Sci 2007; 48:5339-51.
12. Chen TC, Zeng A, Sun W, Mujat M, de Boer JF. Spectral domain optical coherence tomography and glaucoma. Int Ophthalmol Clin 2008; 48:29-45.
13. Testoni PA, Mangiavillano B. Optical coherence tomography in detection of dysplasia and cancer of the gastrointestinal tract and bilio-pancreatic ductal system. World J Gastroenterol 2008; 14:6444-52.
14. Suter MJ, Vakoc BJ, Yachimski PS, Shishkov M, Lauwers GY, Mino-Kenudson M, et al. Comprehensive microscopy of the esophagus in human patients with optical frequency domain imaging. Gastrointest Endosc 2008; 68:745-53.
15. Hariri LP, Bonnema GT, Schmidt K, Winkler AM, Korde V, Hatch KD, et al. Laparoscopic optical coherence tomography imaging of human ovarian cancer. Gynecol Oncol 2009; 114:188-94.
16. Brewer MA, Utzinger U, Barton JK, Hoying JB, Kirkpatrick ND, Brands WR, et al. Imaging of the ovary. Technol Cancer Res Treat 2004; 3:617-27.
17. Boppart SA, Bouma BE, Pitris C, Tearney GJ, Fujimoto JG, Brezinski ME. Forward-imaging instruments for optical coherence tomography. Opt Lett 1997; 22:1618-20.
18. Boppart SA, Goodman A, Libus J, Pitris C, Jesser CA, Brezinski ME, et al. High resolution imaging of endometriosis and ovarian carcinoma with optical coherence tomography: feasibility for laparoscopic-based imaging. Br J Obstet Gynaecol 1999; 106:1071-7.
19. Feldchtein F, Gelikonov G, Gelikonov V, Kuranov R, Sergeev A, Gladkova N, et al. Endoscopic applications of optical coherence tomography. Opt Express 1998; 3:257-70.
20. Sergeev A, Gelikonov V, Gelikonov G, Feldchtein F, Kuranov R, Gladkova N, et al. In vivo endoscopic OCT imaging of precancer and cancer states of human mucosa. Opt Express 1997; 1:432-40.
21. Escobar PF, Rojas-Espaillat L, Tisci S, Enerson C, Brainard J, Smith J, et al. Optical coherence tomography as a diagnostic aid to visual inspection and colposcopy for preinvasive and invasive cancer of the uterine cervix. Int J Gynecol Cancer 2006; 16:1815-22.
22. Zuluaga AF, Follen M, Boiko I, Malpica A, Richards-Kortum R. Optical coherence tomography: a pilot study of a new imaging technique for noninvasive examination of cervical tissue. Am J Obstet Gynecol 2005; 193:83-8.
23. Escobar PF, Belinson JL, White A, Shakhova NM, Feldchtein FI, Kareta MV, et al. Diagnostic efficacy of optical coherence tomography in the management of preinvasive and invasive cancer of uterine cervix and vulva. Int J Gynecol Cancer 2004; 14:470-4.
24. Gossage KW, Tkaczyk TS, Rodriguez JJ, Barton JK. Texture analysis of optical coherence tomography images: feasibility for tissue classification. J Biomed Opt 2003; 8:570-5.
25. Pitris C, Goodman A, Boppart SA, Libus JJ, Fujimoto JG, Brezinski ME. High-resolution imaging of gynecologic neoplasms using optical coherence tomography. Obstet Gynecol 1999; 93:135-9.
26. Kuranov RV, Sapozhnikova VV, Shakhova NM, Gelikonov VM, Zagainova EV, Petrova SA. Combined applications of optical methods to increase the information content of optical coherent tomography in diagnostic of neoplastic processes. Quantum Electron 2002; 32:993-8.
27. Ramanujam N. Fluorescence spectroscopy of neoplastic and non-neoplastic tissues. Neoplasia 2000; 2:89-117.
28. Thekkek N, Richards-Kortum R. Optical imaging for cervical cancer detection: solutions for a continuing global problem. Nat Rev Cancer 2008; 8:725-31.
29. Cardenas-Turanzas M, Freeberg JA, Benedet JL, Benedet JL, Atkinson EN, Cox DD, et al. The clinical effectiveness of optical spectroscopy for the in vivo diagnosis of cervical intraepithelial neoplasia: where are we? Gynecol Oncol 2007; 107:138-46.
30. Freeberg JA, Benedet JL, West LA, Atkinson EN, MacAulay C, Follen M. The clinical effectiveness of fluorescence and reflectance spectroscopy for the in vivo diagnosis of cervical neoplasia: an analysis by phase of trial design. Gynecol Oncol 2007; 107:270-80.
31. Drezek RA, Richards-Kortum R, Brewer MA, Feld MS, Pitris C, Ferenczy A, et al. Optical imaging of the cervix. Cancer 2003; 98:2015-27.
32. Brewer M, Utzinger U, Silva E, et al. Fluorescence spectroscopy for in vivo characterization of ovarian tissue. Lasers Surg Med 2001; 29:128-35.
33. Brewer M, Utzinger U, Li Y, Gershenson D, Bast RC Jr, Follen M, et al. Fluorescence spectroscopy as a biomarker in a cell culture and in a nonhuman primate model for ovarian cancer chemopreventive agents. J Biomed Opt 2002; 7:20-6.
34. Brewer M, Utzinger U, Satterfield W, Hill L, Gershenson D, Bast R, et al. Biomarker modulation in a nonhuman rhesus primate model for ovarian cancer chemoprevention. Cancer Epidemiol Biomarkers Prev 2001; 10:889-93.
35. Kanter EM, Walker RM, Marion SL, Brewer M, Hoyer PB, Barton JK. Dual modality imaging of a novel rat model of ovarian carcinogenesis. J Biomed Opt 2006; 11:041123.
36. Tumlinson AR, Hariri LP, Utzinger U, Barton JK. Miniature endoscope for simultaneous optical coherence tomography and laser-induced fluorescence measurement. Appl Opt 2004; 43:113-21.
37. Kurman RJ, Shih Ie M. Pathogenesis of ovarian cancer: lessons from morphology and molecular biology and their clinical implications. Int J Gynecol Pathol 2008; 27:151-60.
38. Hariri LP, Tumlinson AR, Besselsen DG, Utzinger U, Gerner EW, Barton JK. Endoscopic optical coherence tomography and laser-induced fluorescence spectroscopy in a murine colon cancer model. Lasers Surg Med 2006; 38:305-13.
39. Nadiarnykh O, LaComb RB, Brewer MA, Campagnola PJ. Alterations of the extracellular matrix in ovarian cancer studied by second harmonic generation imaging microscopy. BMC Cancer 2010; In press.
40. Young RH, Scully RE. Sex cord-stromal, steroid cell and other ovarian tumors. In: Kurman R, editor. Blaustein's pathology of the female genital tract. 5th ed. New York: Springer-Verlag 2002; 905-66.

©2010 Landes Bioscience. Do not distribute.